Steel and Composite Structures, Vol. 11, No. 3 (2011) 233-250
DOI: http://dx.doi.org/10.12989/scs.2011.11.3.233

Shear bond failure in composite slabs – a detailed experimental study

Shiming Chen*, Xiaoyu Shi, and Zihao Qiu

School of Civil Engineering, Tongji University, Shanghai 200092, People's Republic of China

(Received July 28, 2010, Accepted April 14, 2011)

Abstract An experimental study has been carried out to reveal the shear-bond failure mechanism of composite deck slabs. Thirteen full scale simply supported composite slabs are studied experimentally, with the influence parameters like span length, slab depth, shear span length and end anchorage provided by steel headed studs. A dozen of strain gauges and LVDTs are monitored to capture the strain distribution and variation of the composite slabs. Before the onset of shear-bond slip, the longitudinal shear forces along the span are deduced and found to be proportional to the vertical shear force in terms of the shear-bond strength in the m-k method. The test results are appraised using the current design procedures. Based on the partial shear-bond connection at the ultimate state, an improved method is proposed by introducing two reduction factors to assess the moment resistance of a composite deck slab. The new method has been validated and the results predicted by the revised method agree well with the test results.

keywords: composite slabs, shear bond failure, load carrying capacity, design method

1. Introduction

The composite floor system consisting of profiled steel sheeting and concrete is now widely used in buildings all over the world. Favorable application of this kind of floor system is resulted from the great advantages such as no form work, quick installation, reduced dimensions and weight to the construction of building floors. In most cases, the behaviors of composite slabs are governed by the horizontal shear bond at the interface between the steel deck and the concrete, and the shear bond failure mechanism of the composite slabs likely depends on the properties of steel deck and concrete as well as that of the interface.

To reveal the shear bond behavior of composite slabs, significant studies were conducted by Porter and Ekberg (1976), upon which an empirical design equation for the shear bond strength was developed based on the linear regressions of the test data on a series of full scale performance tests of composite slabs. The method was further verified and supported by many other researchers (Wright et al 1987, Jolly and Zubair 1987, Wright 1998). The design procedures of the longitudinal shear for composite slabs with profiled steel sheeting, such as the *m-k* and the partial shear connection (τ_u) methods are deduced essentially from the full scale one-way span bending tests (EUROCODE 4 2004, ANSI/ AASCE3-91 1992). Using these design procedures, the number of tests needed to determine the

* Corresponding author, Professor, E-mail: chensm@mail.tongji.edu.cn

behavior of the various existing commercial products under the service and the ultimate loading becomes numerous. This would result in considerable rise of the pecuniary and time costs. Besides, due to the semi-empirical nature of these two methods, neither model illustrates a clear picture of the physical mechanism of the steel-concrete shear bond connection. In the *m-k* method, the shear bond strength V, in terms of the vertical shear force also includes the geometric parameters like the cross section area of steel sheet, so that it is not simply a shear bond resistance inherent at the interface. As an alternative to the *m-k* method, the τ_u method is proposed only for the ductile composite slabs. To determine the maximum shear stress τ_u, the shear span should be sufficient slender provided that the longitudinal shear failure would occur.

Over the last few decades, a number of full scale bending tests have been carried out (Easterling and Young 1991, Chen 2003, Vainiûnas 2006, Marimuthu et al 2007). Most of the tests were committed to provide data to enable the linear regression equation for the ultimate strength of composite slabs with the typical steel profiles. The aspects like the shear bond stress distribution over the span and initiation of the shear bond failure at the steel-concrete interface, which are crucial in governing of shear bond mechanism, and should influence the shear bond behavior of the composite floor, however are still not well measured and understood.

The shear-bond strength is an inherent property for each specific composite slab as far as the steel profiles and the concrete are the same. Attempts have been made to develop new design methods for composite slabs based on the idea of using experimental values from small-scale tests instead of the standard large-scale tests (Daniels and Crisinel 1993, Abdullah and Easterling 2007). Jeong (2008) also proposed a simplified model for the partial-interactive structural performance of steel–concrete composite slab. Lopes E. and Simões R. (2008) presented a "New Simplified Method" based on pull-out tests, attempted a valid alternative to the EUROCODE 4 method. A new element test method for composite slab specimens under bending was presented by Abdullah and Easterling (2009), in which the narrow specimen cutting from a whole composite slab specimen had a width equal to one rib of a typical trapezoidal deck profile, while the other dimension of this narrow specimen was the same as the that in the full scale tests, and the influence as well as the defined shear span slenderness be recognized as a major contributor to the shear bond behavior was discussed by Chen(2010).

The aim of this research is to reveal the shear-bond failure mechanism of composite deck slabs. An experimental study on shear-bond failure mechanism of composite deck slabs has been conducted. Two groups of 13 composite deck slabs were designed and studied experimentally. Strains of the concrete and the steel sheeting along the span length and slab depth are measured and are used in assessing the shear-bond mechanism of the composite deck slabs. Distribution of the longitudinal shear stress along span is also derived from the test results. A new method is proposed to assess the moment resistance of a composite deck slab. The new method has been validated and the calculation results of the composite slabs predicted by the revised method agree well with the test results.

2. Test program

Thirteen full scale composite slabs were designed and tested thoroughly, among which eight specimens were composite slabs without end anchorage, and five specimens were slabs with end anchorage. The all slabs were single-span and monotonically loaded. As the maximum capable shear-bond force is an inherent property for each specific composite slab as far as the steel profile and the concrete are the same, the primary variables considered in the test program were shear span length, and

end restraints. Influence factors like span length, slab depth were also considered in the test.

The steel profile used is 3W-DECK, which is trapezoidal shaped. Geometric shape of the 3W-DECK is illustrated in Fig. 1, and the properties of the profile are listed in Table 1.

The elevation and specimen details of the test program are shown in Fig. 2. Numbering of specimens with variable details for each composite slab is given in Table 2.

As shown in Table 2, the shear span lengths range from 0.41 m to 1.5 m, in terms of the shear span slenderness L_s / d_p from 4.2 to 15.5. $L / 4$ shear span length was adopted for most of the specimens except for slabs 1, 2, 3 and 6, where $L / 4$ shear span should be a simulation of the shear span when the uniform load applied to the entire span length in most cases of the building floors.

In the specimens with end restraints, the end anchorages were provided by steel headed studs, 19 mm in diameter, welded through the steel sheeting to the top flange of the supported steel beam. Two arrangements of stud were adopted in the study, one is one stud per trough, and the other is two studs in row longitudinal per trough.

Concrete was cast in a fully supported condition for the specimens without end anchorage. For the specimens with end restraints to the supported beams, concrete was cast with one-third and mid-span props in cases of span equal to 4 m and 2.5 m respectively. The light steel fabric, 5.5 mm in diameter and 200 mm in spacing, was placed 20 mm from the top of concrete slab. The mean concrete cubic strength at 28 days is 25 N/mm^2.

Fig. 3 shows the rigs of the test program. The all slabs were loaded by a hydraulic jack system. The load was exerted to the specimen via the two distribution beams.

All of the tests were similarly instrumented (Fig. 3). Eight displacement transducers (LVDT) were monitored underneath the quarter span, mid-span and etc. along the span to get the full deflection curves for each slab. Two LVDTs were monitored each end of the slab to catch the relative end slip between the steel deck and the concrete. Concrete strains were measured by strain gauges monitored in the top of concrete slabs, steel wires embedded in concrete over depth and along span for each slab. Strains of the headed studs were monitored, and the two strain gauges were affixed to the shank sides of

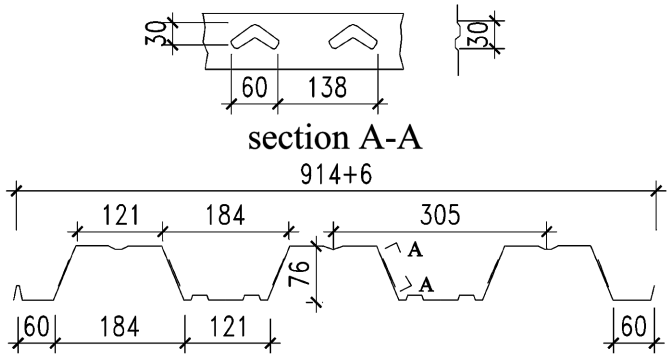

Fig. 1 Geometric shape of 3W-DECK

Table 1 Geometry and strength properties of the 3W- DECK

Thickness t_p (mm)	Area A_p (mm^2)	Weight (kg/m)	Width (mm)	I_x(×10^6) mm^4	f_p (N/mm^2)	f_u (N/mm^2)
0.9	1170.8	9.188	914	1.152	275	380

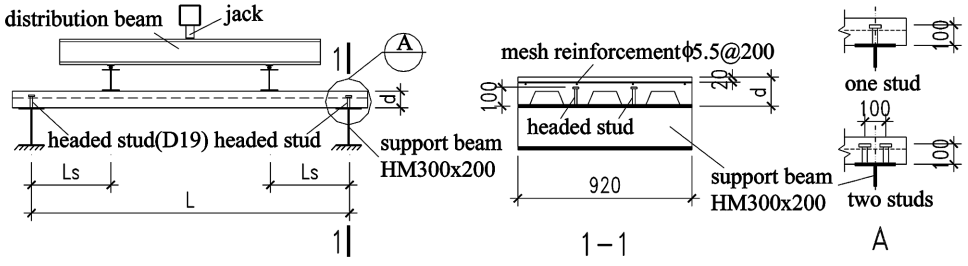

Fig. 2 Test arrangement and specimen details

Table 2 Details of tested composite slabs

No.	Span L/m	Slab thickness d/mm	Shear span L_s/mm	Slenderness L_s/d_p	End anchorage (per trough)
1	2.5	135	410	4.2	none
2	2.5	135	725	7.5	none
3	2.5	135	950	9.8	none
4	4.0	135	1000	10.3	none
5	4.0	135	1000	10.3	none
6	4.0	135	1500	15.5	none
7	2.5	165	625	4.9	none
8	4.0	165	1000	7.9	none
9	2.5	135	625	6.4	one stud
10	2.5	165	625	4.9	one stud
11	2.5	135	625	6.4	two studs
12	4.0	135	1000	10.3	one stud
13	4.0	165	1000	7.9	one stud

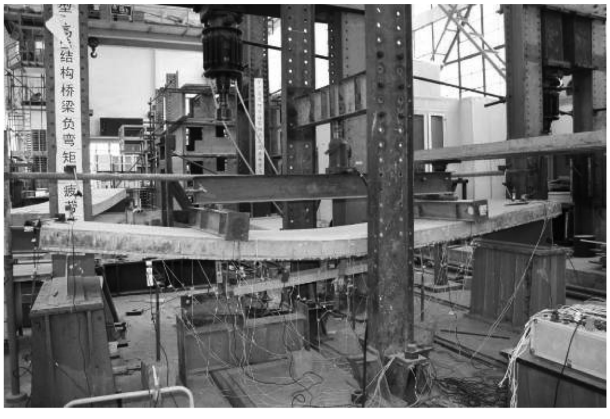

Fig. 3 Test rigs and monitored LVDTs

each steel stud in such a way that in-plane bending of the stud could be detected. Strain gauges were also monitored on the top, the web and the bottom flange of the steel profile along the span to get detailed strain distribution of the steel deck.

The specimens were all monotonically loaded with an initial increment of loading 2 or 3 kN for those

specimens without end anchorage and and 5 to 10 kN for those specimens with end anchorage. The slabs were then loaded gradually up to the maximum load. The tests were terminated when the load dropped by 20% from the maximum, or when the mid-span deflections were close to 1/50 of the span. All electric digital data were collected using the data logger, controlled by a PC computer.

3. Test results and discussion

3.1 Behavior of composite slabs

During the tests for the all slabs, with increase of loading, slight debonding cracking between steel sheeting and concrete was heard before visible cracks were observed in concrete slabs. Fine cracks initiated at the bottom of concrete near the load points and subsequently debonding slips occurred at the interface between the steel deck and the concrete. Subsequent cracks occurred and developed upward to the top of concrete as the loading increased.

Both brittle and ductile failures were observed for the specimens without end anchorage. For specimens failing in brittle failure, after initial fine cracks occurred underneath the load points, few subsequent cracks developed rapidly in midspan of the slabs, accompanying with a rapid developing end slip observed and the specimens failed featuring by the loading dropping sharply. For specimens failing in ductile behavior, after initial end slip occurring, more subsequent fine cracks developed in the midspan as the loading being sustained. The specimens would fail when the load dropped down by 20%, or when the end slip equaled to 0.1 mm. Load-deflection curves of the specimens without end anchorage are drawn in Fig. 4.

For specimens restrained by the end anchorage or headed studs, ductile behaviors were observed. Similar debonding cracking was heard in early stage of loading, then cracks of concrete initiated near the load points. As the load continued increasing, subsequent fine cracks were observed in the concrete slabs between the two load points. In most cases, the first relative end slip were detected at the end in the side when the initial crack formed. The loading was sustaining and capable of considerable increase in magnitude before a much louder debonding cracking was heard and more major cracks of concrete were observed. Substantial end slips and deflection developed at the ultimate state of the composite slabs, when the midspan deflections exceed one fiftieth of the span. Fig. 5 showed the load-deflection curves of the specimens with end anchorage.

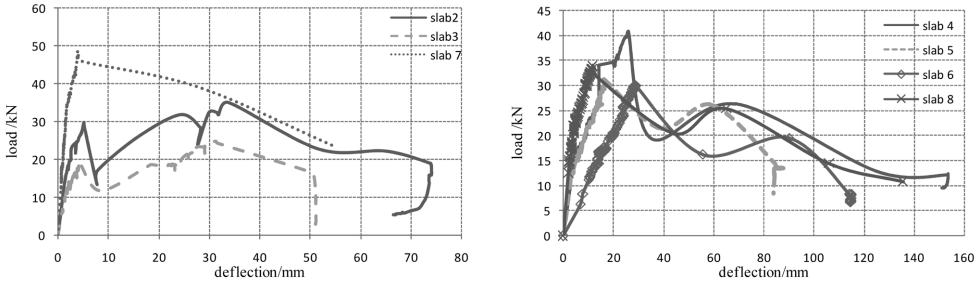

(a) Span of 2500mm (b) Span of 4000mm

Fig. 4 Load-deflection curves of specimens without end anchorage

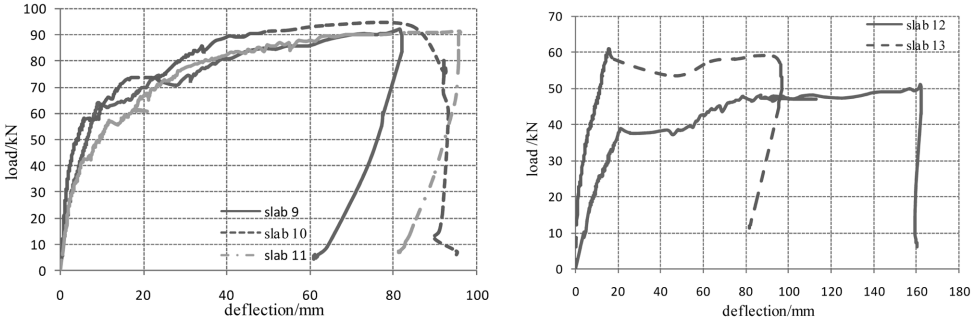

(a) Span of 2500mm (b) Span of 4000mm

Fig. 5 Load-deflection curves of specimens with end anchorage

For the all ductile slabs with end anchorage, fine cracks were observed uniformly distributed approximate 100 mm in spacing mainly in pure bending regions between the two concentrated loads (Fig. 6).

Fig. 7 shows the load-end slip curves of slab 10 and 11, the slabs with end anchorage, where the suffixes *L* and *R* represent the left and the right ends of the slabs.

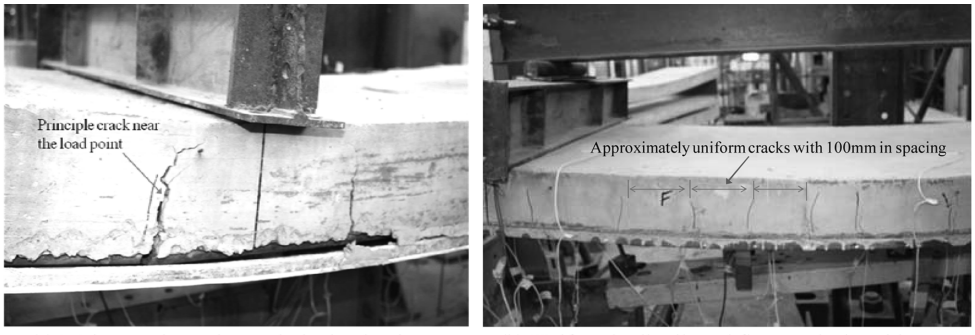

(a) Major cracks underneath the load points (b) Uniformly distributed fine cracks in midspan

Fig. 6 Crack patterns of composite slabs

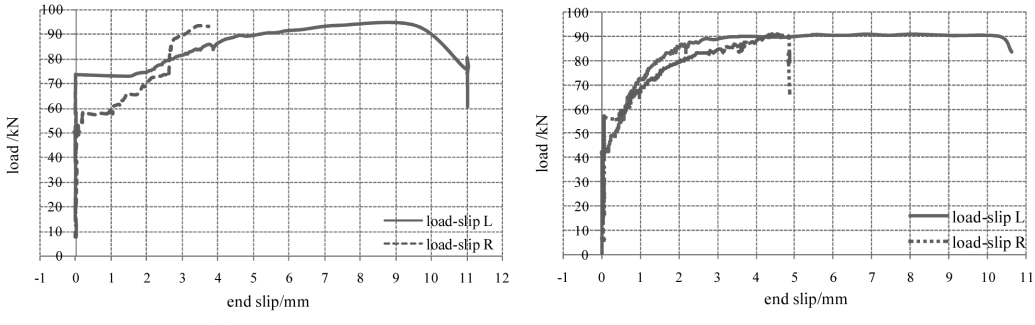

(a) Slab 10 (b) Slab 11

Fig. 7 load-end slip curves of specimens

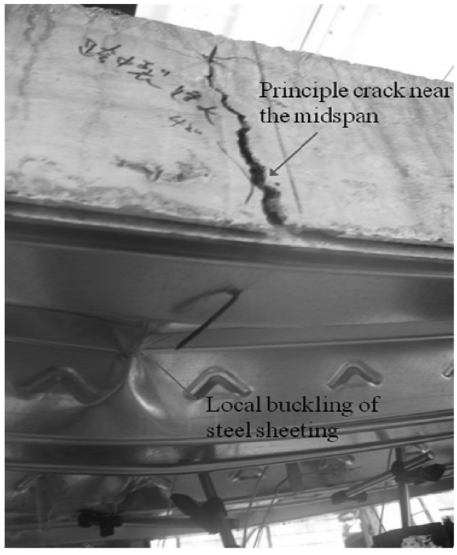

Fig. 8 concrete crack and local buckling of steel sheeting

Local buckling of the top flange and the web of steel deck were also found at the failure state for the all specimens, mainly in midspan region or underneath the load points (Fig. 8). Crushing occurred only in the top of the midspan concrete slab for slab 11(with two end studs per trough). It would be likely that sufficient end restraints provided by the two studs contributed to the shear-bond strength so that to the full developed capacity of composite cross section.

3.2 Summary of load carrying capacities

A summary of the test results expressed as P and M is given in Table 3, in which P and M are the exerted load and the moment at the midspan of each specimen, the subscripts cr, s and u are notated for the initial crack in concrete, the initial shear-bond slip and the maximum load detected in the tests respectively. In Table 3, the slenderness is defined as the ratio of shear span length to the effective depth of the slab L_s / d_p, where d_p is the depth measured from the top of concrete slab to the centroid of the steel deck, M_p is the plastic moment of the cross-section assuming full interaction at the sheet-concrete interface.

In the all tests, the maximum moment (sagging) of each composite slab was found lower than the plastic moment M_p, whatever being end restrained or not, and the slip as well as the vertical separation were observed, so that the strength or the load carrying capacity of the composite slabs were governed by the shear-bond failure at the interface between the steel profiled sheeting and the concrete.

As shown in the final column, the failure pattern of specimens are classified as ductile and brittle in accordance with EUROCODE 4.

The ratio M_u/M_p is plotted aganst L_s/d_p as shown in Fig. 9. It appears that L_s/d_p does not influnece the ratio of M_u/M_p in the cases of slabs with end restraints. For slabs without end anchorage, the larger L_s/d_p implys a larger shear span length, so that a great longitudinal resistance to the shear-bond slip, which leads to a high degree interaction between the steel deck and the concrete.

Table 3 also illustrates the sequence of the mechanism developed in the composite slabs. Firstly,

Table 3 Summary of test results for load carrying capacities

No.	L_s / d_p	P_{cr} / kN	M_{cr} / kN.m	P_s / kN	M_s / kN.m	P_u / kN	M_u / kNm	M_p / kN.m	M_u / M_p	Failure pattern
1	4.2	21.63	4.57	38.11	7.94	56.45	11.70	27.20	0.430	ductile
2	7.5	12.23	4.57	29.02	10.65	35.00	12.82	27.20	0.471	ductile
3	9.8	11.13	5.42	18.72	9.02	24.81	11.92	27.20	0.438	ductile
4	10.3	14.89	7.80	40.86	20.43	40.86	20.43	27.20	0.751	brittle
5	10.3	11.79	6.25	31.24	15.62	31.24	15.62	27.20	0.574	brittle
6	15.5	8.43	6.68	25.64	19.58	30.03	22.87	27.20	0.841	ductile
7	4.9	14.63	4.75	48.52	15.16	48.52	15.16	37.33	0.406	brittle
8	7.9	15.91	8.42	33.97	16.99	33.97	16.99	37.33	0.455	brittle
9	6.4	16.86	5.40	63.90	19.97	84.53	26.42	27.20	0.971	ductile
10	4.9	15.81	5.11	49.05	15.33	91.28	28.52	37.33	0.764	ductile
11	6.4	17.40	5.57	42.52	13.29	85.92	26.85	27.20	0.987	ductile
12	10.3	13.39	7.05	38.83	19.42	47.49	23.75	27.20	0.873	ductile
13	7.9	16.55	8.74	60.91	30.46	60.91	30.46	37.33	0.816	brittle

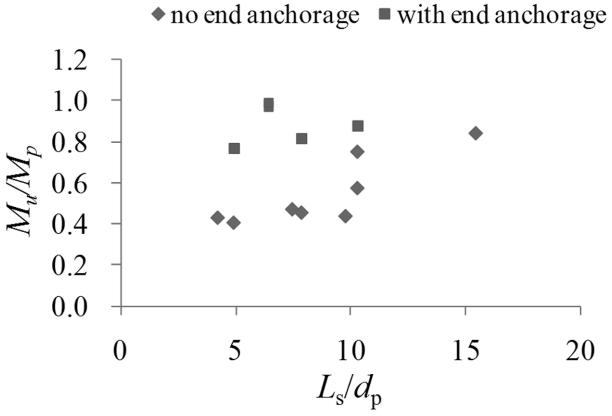

Fig. 9 Influence of L_s / d_p on M_u / M_p

chemical debonding initiated, featuring by cracking sound, then cracks in concrete slab occurred, starting from the bottom of concrete slab underneath the loading positions; and then the relative slip and separation occurred and developed at the interface featuring by mechanical interlock action between the steel deck and the concrete; finally, the major slips and cracks in concrete occurred, the load dropped and slabs failed.

Compared with the specimens without end anchorage, the load carrying capacities of the composite slabs with end restraints are all substantially increased.

3.3 Strain (stress) distribution and shear-bond mechanism

To reveal the shear-bond mechanism, dozens of strain gauges were monitored in the concrete and in the steel deck along the span and over the slab depth. Strains of a rebar embedded in concrete slab along

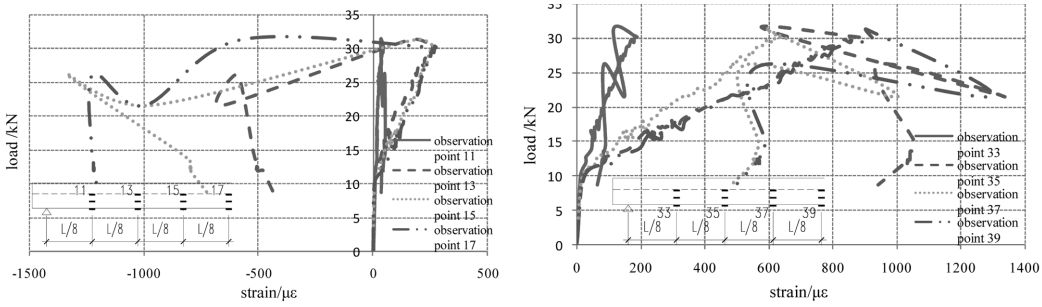

(a) Strain in concrete (b) Stain of the bottom of steel deck

Fig. 10 load-strain curves of steel sheeting at various positions for slab 5

the span length (at positions 11, 13, 15 and 17) are plotted against the applied load in Fig. 10 (a), and the strains of the steel bottom flange at the positions 33, 35, 37 and 39 are plotted in Fig. (b) for slab 5.

From the curves of strains varying with the exerted load, it is illustrated that before cracking of concrete, the concrete portion was in tension, then there were rapid strain increases in concrete when cracks initiated at a load of 11.8 kN, and the concrete sharply changed to compression at a load around 32 kN when slip s were detected at the end of the slab. Similar strain increases in the bottom of steel deck were also detected when cracks initiated, and sharp increases of tensile strain in the steel deck when the end slips occurred.

Based on the stress-strain relationship of the steel, the stress is derived from the measured strain. The stress distributions of the steel profile along the span are shown in Fig. 11(slab 5, without end stud anchorage). It is illustrated that the bottom flanges of the steel deck were all subjected to tension stress from the beginning to the ultimate state, while the top flanges of the steel deck changed from being stressed in tension before initiation of slip between the concrete and the deck to being stressed fully in compression at the ultimate state in the all specimens.

The shear-bond stress at the interface can be deduced by equilibrium of the segment of the steel flanges (top and bottom). An important feature is found that before cracking in concrete, the shear-bond stress exists only in the shear span region, and no shear-bond stress occurs in the midspan region which is in pure bending with a uniform tensile stress distribution for the composite slabs. After that, shear-bond stresses occur in the midspan, both in the top and the bottom flanges. This testing finding verifies

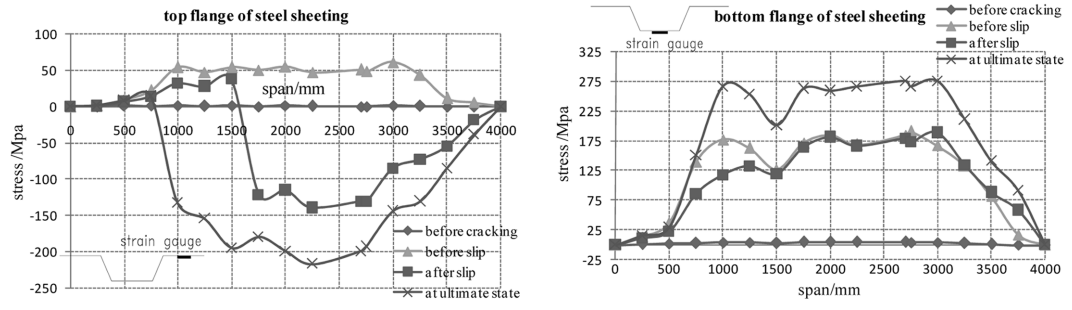

Fig. 11 Stress distribution of steel sheeting along span length for slab 5

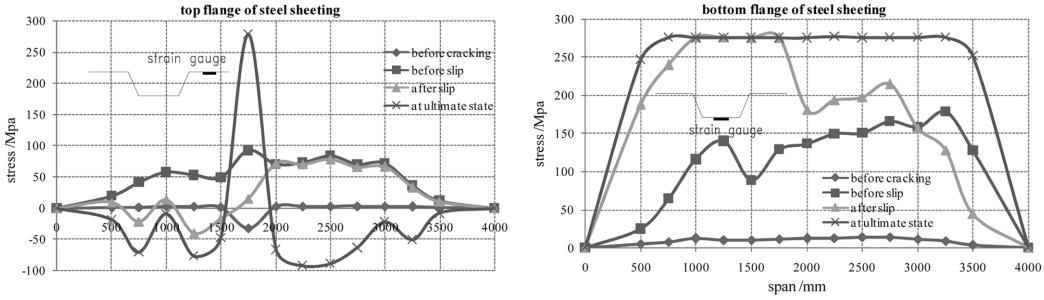

Fig. 12 Stress distribution of steel sheeting along span length for slab 12

that shear bond is a property of the steel-concrete interface. After flexural cracking of the mid-span concrete, there would be a minor relative slip between the concrete and the steel and a discrete strain occurs in concrete adjacent the cracks, which contribute to a shear bond stress at the interface.

Fig. 12 illustrates stress distributions of the steel profile along the span for slab 12 for different loading states. Similar stress distributions were observed in slabs with end stud anchorage. A comparison of load-strain curves at the midspan section for slab 5 and slab 12 is shown in Fig. 13. It is verified that end anchorage of headed studs could restrain the separation and the slip between the steel deck and the concrete, so that the load when shear-bond slip occurs and the ultimate load of the composite slabs increase greatly.

As shown in Figs. 10, 11, 12 and 13, the stress of steel sheeting have significant changes when relative slip commences at the steel-concrete interface. Prior to initiation of slip, the whole steel profile is in tension. After initiation of slip, some parts of the top flange of steel profile turn into compression due to the localized separation at the interface, and the bottom flange and most of the web of steel sheeting are still in tension. At the ultimate failure state, local buckling occurs in the top flange and in the major parts of web of steel sheeting, and the bottom flange of steel sheeting stressed in tension reaches its yielding strength.

It is concluded that the shear-bond slip plays the dominant role. After commencement of the relative slip, the full component interaction at the steel-concrete interface is weaken and replaced by partial shear-bond slip interaction.

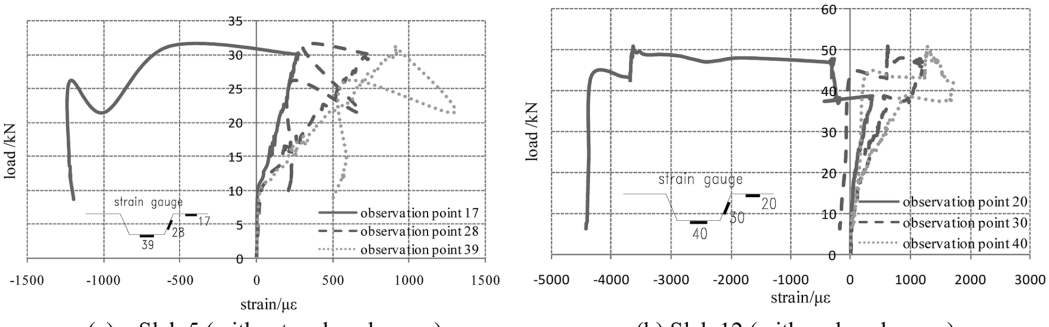

(a) Slab 5 (without end anchorage) (b) Slab 12 (with end anchorage)

Fig. 13 Load vs. strains of the steel sheeting at the mid span section

3.4 Analysis of the longitudinal shear

Abdullah and Easterling (2007) proposed a calculation procedure to generate shear-bond stress versus slip relationship from bending tests. The method is modified and the measured strain distributions over the cross section sections are used in determination of the changing moment arm, z. A segment of composite slab is taken out for analysing the longitudinal shear force. Accordingly, the strain distribution and the internal forces actiong on the cross-section of a composite slab are shown in Fig. 14. Neglecting the self-weight, by equilibrium, the longitudinal shear force, F acting at the steel-concrete interface can be derived and expressed as

$$F = N_s = \frac{\frac{P}{2}L_s - M_r}{z} \tag{1}$$

where N_s is the longitudinal tensile force of steel sheeting, N_c the compressive normal force acting on the concrete flange, z moment arm between tension and compression force, M_r the remaining moment resistance of the steel deck.

The changing moment arm, z is derived from the strain distribution along the section by

$$z = h - \frac{1}{3}(y_{cc} + y_{ss}) \tag{2}$$

$$y_{cc} = \frac{x_1}{x_1 + x_2}h_c \tag{3}$$

$$y_{ss} = \frac{x_4}{x_3 + x_4}h_s \tag{4}$$

where, y_{cc} is the compression depth of concrete, y_{ss} the tension height of the steel sheeting, the effective depth h_c, is the distance from the top flange of steel sheeting to the top surface of concrete, h_s the height of steel sheeting, h the total depth of the composite slab, x_1, x_1, x_3 and x_4 are the strain of the steel sheeting and concrete respectively as shown in Fig. 14(b) and (c).

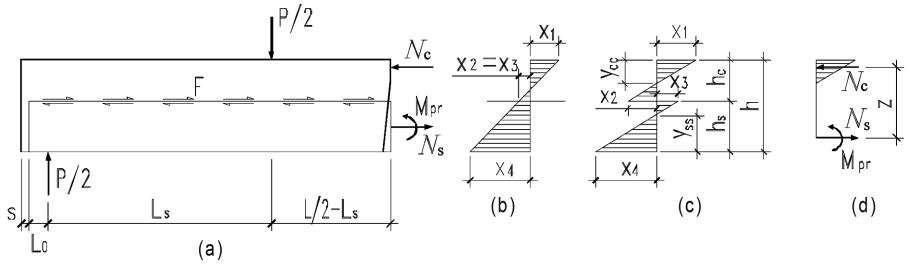

Fig. 14 Segment equilibrium and cross section analysis (a) Segment of a slab (b) strain distribution of cross section before slip (c) strain distribution of cross section after slip (d) equilibrium of internal force

The moment resisted by steel sheeting can be determined by the moment-curvature relationship

$$M_r = \frac{1}{R} E_s I_s \tag{5}$$

where, E_s and I_s are the modulus of elasticity and moment of inertia of the steel deck respectively. If no uplift separation between the steel deck and the concrete, by geometric relationship shown in Fig. 15, the curvature of the steel deck $1/R$ at the position, distant x from the support point is determined by

$$\frac{1}{R} = \frac{\delta_x}{x\left(\frac{L}{2} - x\right)} \tag{6}$$

Using the deflections and the loads exerted measured in the test, the longitudinal shear force at the interface of each cross section along the span can be determined. So that in this way, it is the longitudinal shear force rather than the vertical shear force for each composite slab can be evaluated.

During the test for each specimen, six displacement transducers (LVDTs) were located along the span and two LVDTs at the support to measure the deflections of the composite slab. By polynomial fitting method, these measured deflections were used to determine the deflection curves at the different loading state.

The measured deflections and the load data are put into previous Equations. (Eq. 1 to 6), and the

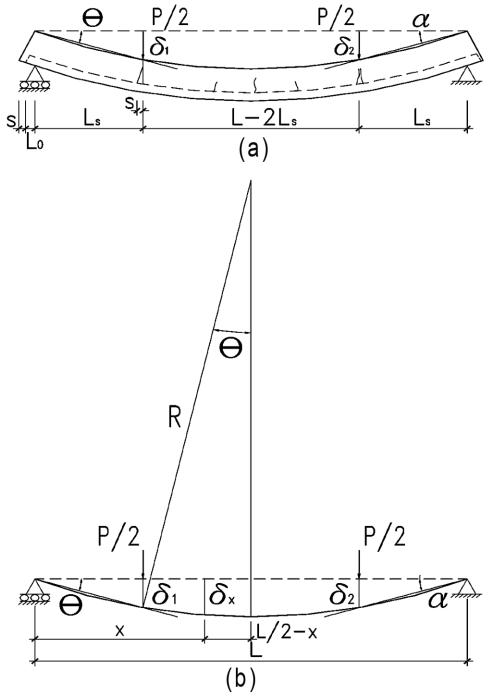

Fig. 15 Curvature and deflection of a slab in bending (a) Deflection mode of the slab (b) Deflection and curvature

longitudinal shear forces at the interface are calculated. Assuming the longitudinal shear force is also uniformed distributed transversely in each sub-segment, notated by i along the slab span, the longitudinal shear-bond stress τ_i is then determined by

$$\tau_i = \frac{N_{si}}{A_{\text{con}i}} \tag{7}$$

where, N_{si} and τ_i are the longitudinal shear-bond force and stress at the cross section (corresponding to the detected deflection) along the span, A_{coni} the contact area of the interface between the steel sheeting and the concrete of each sub-segment.

The longitudinal shear forces distributed over the span length are depicted in Fig. 16 for slab 5 and in Fig. 17 for slab 12, where slab 5 is a composite slab without end anchorage restraints, and slab 12 is a composite slab with end anchorage.

For specimens like slab 5 failed in a brittle pattern, the maximum longitudinal shear force occurred before initiation of the end slips, and the shear force then dropped sharply after commence of the end slip. For specimens with a ductile behavior, however, the longitudinal shear force is capable of further increase after initiation of the end slips, especially for the specimen with end anchorage, like slab 12, the longitudinal shear force continued increasing after commence of the slip.

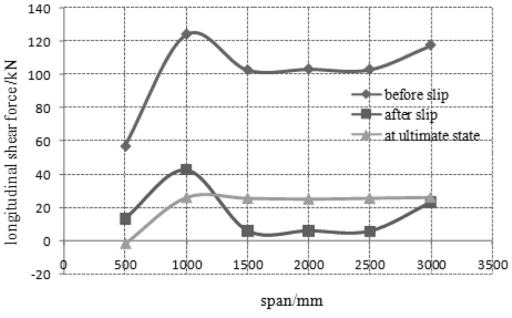

(a) Longitudinal shear force

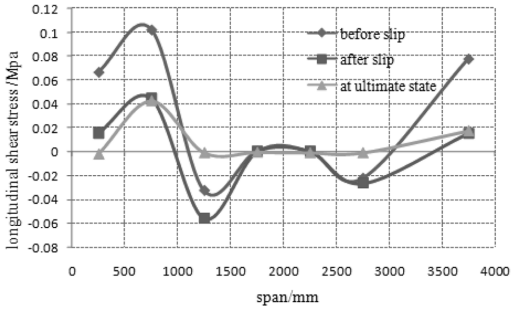

(b) Longitudinal shear-bond stress

Fig. 16 Longitudinal shear force distribution for slab 5

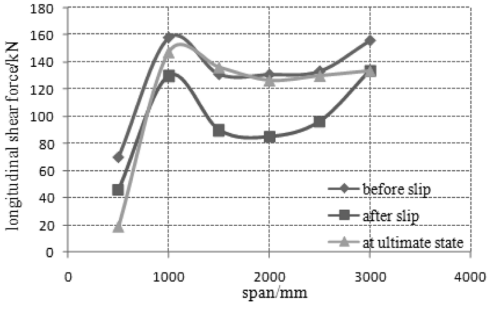

(a) Longitudinal shear force

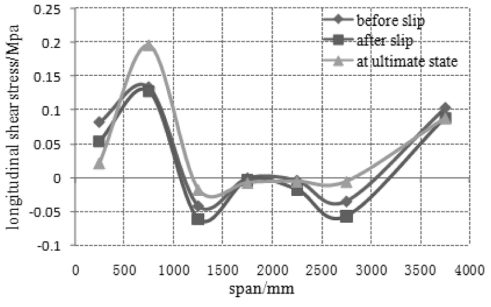

(b) Longitudinal shear-bond stress

Fig. 17 Longitudinal shear force distribution for slab 12

Distribution of shear-bond stress over the whole span is also derived and illustrated in Fig. 16(b) for slab 5 and in Fig. 17 for slab12(b). It appears that the shear-bond stress is not simply uniformed distributed within the shear span as well as in the pure bending region, especially when the slab is beyond elastic and crack stage. The maximum longitudinal shear stress occurs near the load point, while the shear stress distributed between the two exerted load points is much less than that in the shear span. The longitudinal shear-bond stress over the shear span plays dominant contribution to the shear-bond strength for a composite slab. The longer the shear span length is, the more the longitudinal shear-bond resistance would be.

The longitudinal shear force of the cross section where the maximum longitudinal shear occurs appears proportional to the vertical shear force at the support before the onset of end slips as shown in Fig. 18, for typical slabs like slab 5, slab 6 and slab12. For slabs with end anchorage (slab 12), extra longitudinal shear-bond strength is capable to develop in existence of the end stud anchorage.

A linear regression is made for V_L, the maximum longitudinal shear force, and the shear-bond strength in terms of the vertical shear force expressed as

$$V_L = n\frac{L_s}{d_p}V_u \tag{8}$$

Where V_u is the shear-bond strength or the maximum vertical force (adopted in the m-k method), L_s/d_p is the shear span slenderness, and n is a constant, equal to 0.671 in this test

4. An improved method to evaluate the shear bond strength

In the τ_u method (EUROCODE 4 2004), the maximum longitudinal shear stress, τ_u, is expressed as

$$\tau_u = \frac{\eta N_{cf}}{b(L_s + L_0)} \tag{9}$$

where, η is the degree of shear connection, which can be determined from the partial interaction

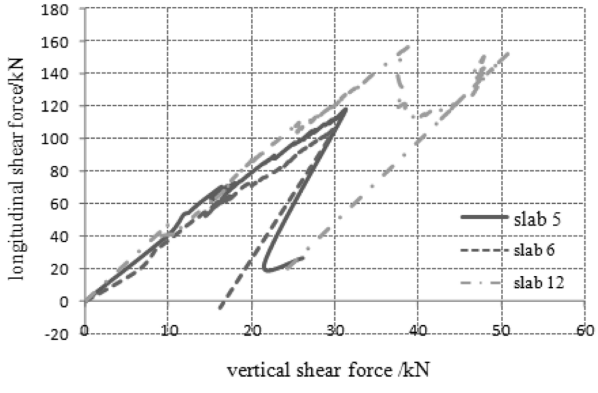

Fig. 18 Longitudinal shear force vs. vertical shear force

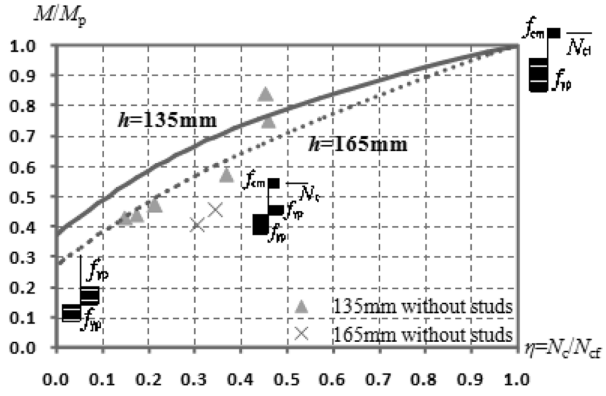

Fig. 19 partial interaction curves for the specimens with various slab depth

diagram as shown in Fig. 19, N_{cf} the compressive normal force in the concrete flange with full shear connection ($\eta = 1$), N_c the compressive normal force in the concrete flange, L_s the shear span and L_0 the length of the overhang.

The moment resistance is expressed as

$$M = N_c z + M_{pr} \tag{10}$$

where, N_c is the compressive normal force in the concrete slab balanced by the tension force in the steel deck, z moment arm between tension and compression force, and M_{pr} the reduced plastic moment of the steel deck.

The longitudinal shear force at the ultimate state is derived from the test measurement of load, strain over the depth as well as deflection for each specimen. The test values of M / M_p and N_c / N_{cf} are then plotted in the partial interactional chart as shown in Fig. 19. It appears that when the partial interaction degree η is lower than 0.4, the τ_u method is overestimate, and the ductile and high partial interaction behavior of the composite slabs are essential required.

Since at the ultimate shear-bond failure state, the bottom steel sheeting would or nearly yield in tension (shown in Fig. 20), the τ method is revised by introducing two reduction factors to assess the moment resistance, and the moment resistance is expressed as

$$M = \eta_1 f_y A_s z / \gamma_{ap} + \eta_2 M_{pa} \tag{11}$$

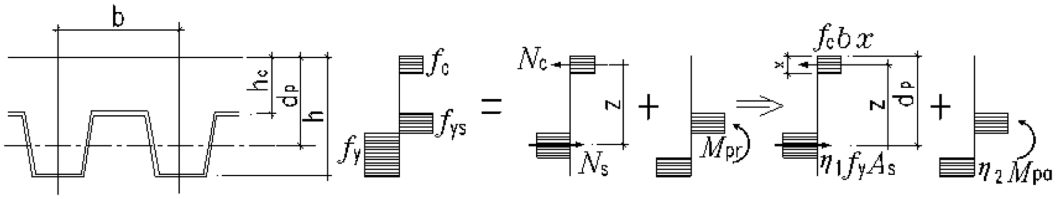

(a) cross-section (b) τ_u method (c) revised method

Fig. 20 Stress distribution of a composite slab in sagging bending

where, η_1 and η_2 are two reduction partial interaction factors, f_y is the yielding strength of steel sheeting, A_s is the cross-section area of the profiled sheeting, M_{pa} the plastic resistance moment of the effective cross-section of the steel sheeting. Lever arm, z, can be calculated by

$$z = d_p - \frac{x}{2} \tag{12}$$

$$x = \frac{\eta_1 f_y A_s / \gamma_{ap}}{0.85 b f_{ck} / \gamma_c} \tag{13}$$

where d_p is the effective depth of the slab, measured from the compression fiber to the steel deck centroid, x the depth in compression of the concrete, f_{ck} characteristic value of the cylinder compressive strength of concrete, γ_{ap} and γ_c are the partial factor for steel sheeting and concrete respectively, 1.1 and 1.5 for γ_{ap} and γ_c in accordance with EUROCODE 4.

Ranges of the reduction factors η_1 and η_2 for each specimen were derived from test results. The recommended values for reduction factors are shown in Table 4. In EUROCODE 4, the longitudinal shear-bond resistance of the slabs with end stud anchorage is determined with N_c increased by the design resistance of the end anchorage, N_r.

The comparison of results calculated by the revised method and test results are shown in Table 5. The test results from Chen (2003) and Marimuthu (2007) are also used to validate the method. From Table 5, it appears that the calculation results predicted by the revised method agree well with the test results. Satisfying results are acquired using the simplified method for the both composite slabs with and without end anchorage restraints.

5. Conclusions

An experimental study on shear-bond failure mechanism of composite deck slabs has been conducted. Shear-bond failures were found for the all specimens, and strains of the concrete and the steel sheeting along the span length and slab depth were measured and were used in assessing the shear-bond mechanism of the composite deck slabs. The conclusions are drawn as the follows:

1. The shear-bond failure mechanism of composite slabs follows the procedure that firstly, the crack of bottom concrete in tension initiates; then the shear-bond slip and separation occurs, and finally the totally loss of shear-bond strength, and the composite deck slabs fail.
2. The longitudinal shear stress does not simply uniformly distribute over the shear span, and it is much smaller within the region between the two load points (or pure bending region) than that in the shear span. So that the longitudinal shear-bond stress among the shear span plays the major contribution to the longitudinal shear-bond strength of a composite deck slab.

Table 4 Recommended values for reduction factors

Specimens	η_1	η_2		
		$L_s / d_p = 0$	$0 < L_s / d_p < 15$	$L_s / d_p = 15$
No end anchorage	0.30	0	$0.0433 L_s/d$	0.65
With end anchorage	0.65		0.40	

Table 5 Comparison of the calculations and the test results

Specimens	No.	Slenderness	Reduction factors		Design moment resistance M / kN.m		M / M_{test}
		L_s / d_p	η_1	η_2	Improved method	Test results	
Present	1	4.23	0.30	0.18	11.18	11.70	0.96
Work	2	7.47	0.30	0.32	12.61	12.82	0.98
	3	9.79	0.30	0.42	13.62	11.92	1.14
	4	10.31	0.30	0.44	13.85	20.43	0.68
	5	10.31	0.30	0.44	13.85	15.62	0.89
	6	15.46	0.30	0.66	16.11	22.87	0.70
	7	4.92	0.30	0.21	14.52	15.16	0.96
	8	7.87	0.30	0.34	15.82	16.99	0.93
	9	6.44	0.65	0.40	23.03	26.42	0.87
	10	4.92	0.65	0.40	29.61	28.52	1.04
	11	6.44	0.65	0.40	23.03	26.85	0.86
	12	10.31	0.65	0.40	23.03	23.75	0.97
	13	7.87	0.65	0.40	29.61	30.46	0.97
Chen	A-1	6.14	0.65	0.40	30.06	31.50	0.95
(2003)	A-2	6.14	0.65	0.40	39.01	42.90	0.91
Marimuthu	1	4.13	0.30	0.18	6.76	8.90	0.76
(2007)	2	4.52	0.30	0.19	6.85	9.13	0.75
	3	4.90	0.30	0.21	6.94	8.99	0.77
	4	10.97	0.30	0.47	8.29	9.61	0.86
	5	12.26	0.30	0.53	8.58	12.79	0.67
	6	14.84	0.30	0.64	9.15	9.42	0.97

3. The longitudinal shear force at the steel-concrete interface derived from the test was found proportional to vertical shear force before the onset of shear-bond slip. The maximum load would be reached when the end-slips initiate for composite slabs without end stud anchorages, while for slabs with end anchorage provided by headed studs, extra substantial strength and ductility would develop after commencement of the end slips.
4. The test results were compared with the current design methods, and it appears that when the partial interaction degree η is lower than 0.4, the τ_u method is overestimate, and the ductile and high partial interaction behavior of the composite slabs are essential required.
5. Based on the partial shear-bond connection at the ultimate state, an improved method is proposed by introducing two reduction factors to assess the moment resistance of a composite deck slab. The new method has been validated and the calculation results of the composite slabs predicted by the revised method agree well with the test results. Satisfying results are acquired using the improved method for the both composite slabs with and without end anchorage restraints.

Acknowledgments

The authors appreciate greatly the National Science Foundation for the partial support for this

research under the Grants No. 50678132, No.51078290 and the support from the Kwang-Hua Fund for College of Civil Engineering, Tongji University. The cooperation and assistance of many people from the organization are greatly acknowledged. The author also acknowledges with thanks the provision of steel work by Far East Steel Structure Engineering (China Co., Ltd.), and the assistance of the technicians at the National Key Laboratory of Disaster Reduction in Civil Engineering of Tongji University.

References

ASCE. Standard for the structural design of composite slabs. ANSI/AASCE3-91. American Society of Civil Engineers. New York, 1992. a)

Abdullah R. and Easterling W. S.(2007), "Determination of composite slab strength using a new element test method," *J. Struct. Eng*. ASCE, **133(9)**, 1268-1277.

Abdullah R. and Easterling W. S.(2009), "New evaluation and modeling procedure for horizontal shear bond in composite slabs," *J. Const. Steel. Res.*, **65(4)**, 891-899.

Chen S. (2003), "Load carrying capacity of composite slabs with various end constraints," *J. Constr. Steel. Res.*, **59(3)**, 385-403.

Chen S. (2010), Discussion of "Determination of composite slab strength using a new element test method", *J. Struct. Eng.* ASCE, **136(8)**, 1032-1034.

Daniels B. J. and Crisinel M.(1993), "Composite slab behavior and strength analysis. Part II: comparisons with test results and parametric analysis," *J. Struct. Eng.* ASCE, **119 (1)**, 16-35.

Eurocode 4: Design of composite steel and concrete structures, Part 1.1:General rules and rules for buildings. EN1994-1-1:2004. European Committee for Standardization. Brussels, 2004

Easterling W. S. and Young C.S. (1991), "Strength of composite slabs," *J. Struct. Eng.* ASCE, **118(9)**, 2370-2389.

Jeong Y.(2008), "Simplified model to predict partial-interactive structural performance of steel-concrete composite slabs," *J. Constr. Steel. Res.*, **64(2)**, 238-246.

Jolly C. K. and Zubair A. K. M.(1987), "The efficiency of shear-bond interlock between profiled steel sheeting and concrete," *Inter. Conference. Steel. Aluminum. Struct.*, Cardiff. London: Elsevier. 127-136.

Lopes E. and Simões R. (2008), "Experimental and analytical behaviour of composite slabs," *Steel. Comp. Struct., An. Int'l. J.*, **8(5)**, 361-388.

Marimuthu V., et al. (2007), "Experimental studies on composite deck slabs to determine the shear-bond characteristic (m-k) values of the embossed profiled sheet," *J. Const. Steel. Res.*, **63(6)**, 791-803.

Porter, M.L. and Ekberg, C. E.(1976), "Design recommendations for steel deck floor slabs," *J. Struct. Div.*, ASCE, **102(11)**, 2121-2136.

Porter, M.L., Ekberg, C.E, Greimann L.F, Elleby H.A.(1976), "Shear-bond analysis of steel-deck-reinforced slabs," *J. Struct. Div.*, ASCE, **102(12)**, 2255-2268.

Vainiûnas P, et al.(2006), "Analysis of longitudinal shear behavior for composite steel and concrete slabs," *J. Constr. Steel. Res.*, **62(12)**, 1264-1269

Wright H.D., Evans H.R., Harding P.W. (1987), "The use of profiled steel sheeting in floor construction," *J. Const. Steel. Res.*, **7(4)**, 279-295.

Wright H. D. (1998), "Composite slabs," *Prog. Struct. Eng. Mater.*, **1(2)**, 178-184.

CC